ADVANCES IN ATMOSPHERIC SCIENCES, VOL. 35, JANUARY 2018, 38–51

• **Original Paper** •

# Remarkable Link between Projected Uncertainties of Arctic Sea-Ice Decline and Winter Eurasian Climate

Hoffman H. N. CHEUNG*[1,2], Noel KEENLYSIDE[1,2,3], Nour-Eddine OMRANI[1,2], and Wen ZHOU[4,5]

[1]*Geophysical Institute, University of Bergen, Bergen* 5007*, Norway*
[2]*Bjerknes Centre for Climate Research, University of Bergen, Bergen* 5007*, Norway*
[3]*Nansen Environmental and Remote Sensing Center, Bergen* 5006*, Norway*
[4]*Guy Carpenter Asia-Pacific Climate Impact Centre, School of Energy and Environment, City University of Hong Kong, Hong Kong, China*
[5]*City University of Hong Kong Shenzhen Research Institute, Shenzhen* 518057*, China*

(Received 22 June 2017; revised 14 September 2017; accepted 26 September 2017)

ABSTRACT

We identify that the projected uncertainty of the pan-Arctic sea-ice concentration (SIC) is strongly coupled with the Eurasian circulation in the boreal winter (December–March; DJFM), based on a singular value decomposition (SVD) analysis of the forced response of 11 CMIP5 models. In the models showing a stronger sea-ice decline, the Polar cell becomes weaker and there is an anomalous increase in the sea level pressure (SLP) along 60°N, including the Urals–Siberia region and the Iceland low region. There is an accompanying weakening of both the midlatitude westerly winds and the Ferrell cell, where the SVD signals are also related to anomalous sea surface temperature warming in the midlatitude North Atlantic. In the Mediterranean region, the anomalous circulation response shows a decreasing SLP and increasing precipitation. The anomalous SLP responses over the Euro-Atlantic region project on to the negative North Atlantic Oscillation–like pattern. Altogether, pan-Arctic SIC decline could strongly impact the winter Eurasian climate, but we should be cautious about the causality of their linkage.

**Key words**: Arctic climate, Siberian high, Icelandic low, three-cell meridional circulation

**Citation**: Cheung, H. H. N., N. Keenlyside, N.-E. Omrani, and W. Zhou, 2018: Remarkable link between projected uncertainties of Arctic sea-ice decline and winter Eurasian climate. *Adv. Atmos. Sci.*, **35**(1), 38–51, https://doi.org/10.1007/s00376-017-7156-5.

## 1. Introduction

Over Eurasia, the wintertime large-scale climatological circulation has two distinct characteristics. First, a dipole pressure pattern, consisting of the Icelandic low and the Azores high, extends zonally over the Euro-Atlantic region. This is strongly linked to the North Atlantic Oscillation (NAO) and the Arctic Oscillation (AO; Thompson and Wallace, 1998). Second, a cold-core surface high is centered over the Siberian–Mongolian region. The Siberian high is the key circulation feature of the East Asian winter monsoon that brings cold air masses equatorward via cold surges (Ding, 1994; Chang et al., 2006). In recent decades, one of the most distinct wintertime circulation features is the warm-Arctic–cold-midlatitude temperature pattern (Cohen et al., 2012; Kug et al., 2015; Sorokina et al., 2016). These temperature changes have motivated more research to study whether and how the Arctic changes and the frequency of extreme weather are connected in the present and the future climate [e.g., see the reviews of Cohen et al. (2014), Vihma (2014), Barnes and Screen (2015) and Gao et al. (2015)]. Specifically, the strengthened Siberian high and the negative NAO/AO contributed to the cold extremes in the Eurasian continent (Honda et al., 2009; Cohen et al., 2012; Kim et al., 2014; Mori et al., 2014; King et al., 2016). However, these circulation changes could be due to the internal climate variability instead of the sea-ice loss (McCusker et al., 2016; Ogawa et al., 2017[a]).

In recent decades, the sea-ice cover has dramatically decreased and this directly affects local heat fluxes and atmospheric circulation (Deser et al., 2010; Screen and Simmonds, 2010). Meanwhile, the Arctic warms faster than other regions and this is called Arctic Amplification (AA; e.g., Graversen et al., 2008). In the late 21st century, when the radiative forcing becomes much stronger than the present climate, the Arctic

* Corresponding author: Hoffman H. N. CHEUNG
Email: Ho.Cheung@uib.no

[a]Ogawa, F., and Coauthors, 2017: Evaluating impacts of the Arctic sea-ice loss on the northern hemisphere climate changes. Submitted.

is expected to become ice-free in summer (Wang and Overland, 2012) and the AA will be stronger. In response to the sea-ice decline and AA, some numerical studies have shown a negative AO-like/NAO-like circulation (e.g., Magnusdottir et al., 2004; Sokolova et al., 2007; Peings and Magnusdottir, 2014; Blackport and Kushner, 2017), and a higher SLP over northern Eurasia (Deser et al., 2016). These circulation changes potentially advect more cold polar air equatorward. However, due to the warmer cold polar air, the AA-related cold-air outbreaks would be weaker than the present climate (Ayarzagüena and Screen, 2016). The thermodynamic effect due to increasing sea surface temperature (SST) would also outweigh the dynamic cooling caused by AA (Deser et al., 2016). The temperature over extratropical Eurasia would generally increase (Deser et al., 2010, 2016) and the probability of cold winters would decrease (Yang and Christensen, 2012), unlike the increasing tendency for the warm-Arctic-cold-midlatitude temperature pattern during the recent AA period (e.g., Cohen et al., 2014).

Although there is high confidence that sea-ice cover will rapidly diminish under future global warming, its rate of retreat has a large intermodel spread across the CMIP5 models (Wang and Overland, 2012). Meanwhile, the midlatitude circulation changes could result from the competing effect of AA and other drivers (Vihma, 2014; Chen et al., 2016; Deser et al., 2016). Thus, the intermodel spread in sea-ice projection could be related to uncertainties in midlatitude atmospheric circulation change. For instance, over North America and the North Atlantic, models disagree on the sign of change of the wintertime midlatitude westerly wind and speed, but the intermodel spread of these quantities is significantly correlated to that of AA (Barnes and Screen, 2015). Through analyzing model outputs from the CMIP5 archive, we address the following questions that have not been analyzed thoroughly by previous studies: (1) What are the projected uncertainties of Arctic sea-ice cover and the Eurasian climate? (2) What is the relationship between these projected uncertainties? (3) Do the models showing a stronger sea-ice decline correspond to cooling or less pronounced warming in any parts of Eurasia?

To answer these questions, we focus on the intermodel spread of the forced response to the Arctic sea-ice decline. To minimize the internal atmospheric variability, we only analyze the 11 CMIP5 models (https://esgf-node.llnl.gov/projects/esgf-llnl/) that include at least three ensemble members for both the historical and RCP8.5 simulations (Table 1). The forced response is regarded as the climatological difference between the period 2069–98 in the RCP8.5 run and 1971–2000 in the historical run; below, we refer to this difference simply as "the response". In each model, the climatology is the unweighted average of all ensemble members listed in Table 1. The multimodel ensemble mean (MME) response is defined by averaging the individual model means. The reason for choosing 2069–98 instead of 2071–2100 is due to some missing outputs in 2099 and 2100. All atmospheric and oceanic variables are interpolated to a horizontal resolution of $2.5^\circ \times 2.5^\circ$ and $1.0^\circ \times 1.0^\circ$, respectively.

## 2. Coherent model uncertainties in the sea-ice–atmosphere response

Before analyzing the coupled linkage between the projected uncertainty of sea-ice cover and the Eurasian circulation, we present the MME and the intermodel standard deviation of the forced response of the sea-ice concentration (SIC) over the Arctic and SLP over Eurasia during boreal winter [December–March (DJFM)] (Fig. 1). Compared to the present climate, the SIC has a robust decline over most of the Arctic in the late 21st century, and this is strongest over the Barents-Kara Sea (> 60%; Fig. 1a). However, the intermodel standard deviation is also large over the Barents-Kara Sea (~ 40%), and its magnitude is comparable to the MME response over large parts of the Arctic (Fig. 1b). This indicates a large uncertainty of ΔSIC in boreal winter, agreeing with the CMIP3 results from Hodson et al. (2013) and the CMIP5 results from Wang and Overland (2012).

Associated with a robust decline in SIC, the SLP consistently decreases over the Arctic in the MME (Fig. 1c). In other polar regions, the strongest SLP decline is over the

**Table 1.** List of the CMIP5 models and their ensemble members used in this study, where "high top" indicates a model with a fully resolved stratosphere with the model top above the stratopause. An asterisk next to the model name indicates the vertical velocity was not available in the archives.

| Number | Model | Ensemble members (r{n}i1p1) | Horizontal resolution of atmospheric model (lat. × lon.) | Horizontal resolution of oceanic model (lat. × lon.) | Model top |
|---|---|---|---|---|---|
| 1 | CanESM2 | 1–5 | $2.8^\circ \times 2.8^\circ$ | $0.9^\circ \times 1.4^\circ$ | Low top |
| 2 | CCSM4 | 1–6 | $0.9^\circ \times 1.3^\circ$ | $0.6^\circ \times 0.9^\circ$ | Low top |
| 3 | CESM1(CAM5) | 1–3 | $0.9^\circ \times 1.3^\circ$ | $0.6^\circ \times 0.9^\circ$ | Low top |
| 4 | CNRM-CM5 | 1, 2, 4, 6, 10 | $1.4^\circ \times 1.4^\circ$ | $0.6^\circ \times 1.0^\circ$ | Low top |
| 5 | CSIRO Mk3.6.0 | 1–10 | $1.9^\circ \times 1.9^\circ$ | $1.9^\circ \times 0.9^\circ$ | Low top |
| 6 | FIO-ESM | 1–3 | $2.8^\circ \times 2.8^\circ$ | $0.5^\circ \times 1.1^\circ$ | Low top |
| 7 | HadGEM2-CC* | 1–3 | $1.3^\circ \times 1.9^\circ$ | $0.8^\circ \times 1.0^\circ$ | High top |
| 8 | HadGEM2-ES* | 1–4 | $1.3^\circ \times 1.9^\circ$ | $0.8^\circ \times 1.0^\circ$ | Low top |
| 9 | IPSL-CM5A-LR | 1–4 | $1.9^\circ \times 3.8^\circ$ | $1.2^\circ \times 2.0^\circ$ | High top |
| 10 | MIROC5 | 1–3 | $1.4^\circ \times 1.4^\circ$ | $0.8^\circ \times 1.4^\circ$ | Low top |
| 11 | MPI-ESM-LR | 1–3 | $1.9^\circ \times 1.9^\circ$ | $0.8^\circ \times 1.4^\circ$ | High top |

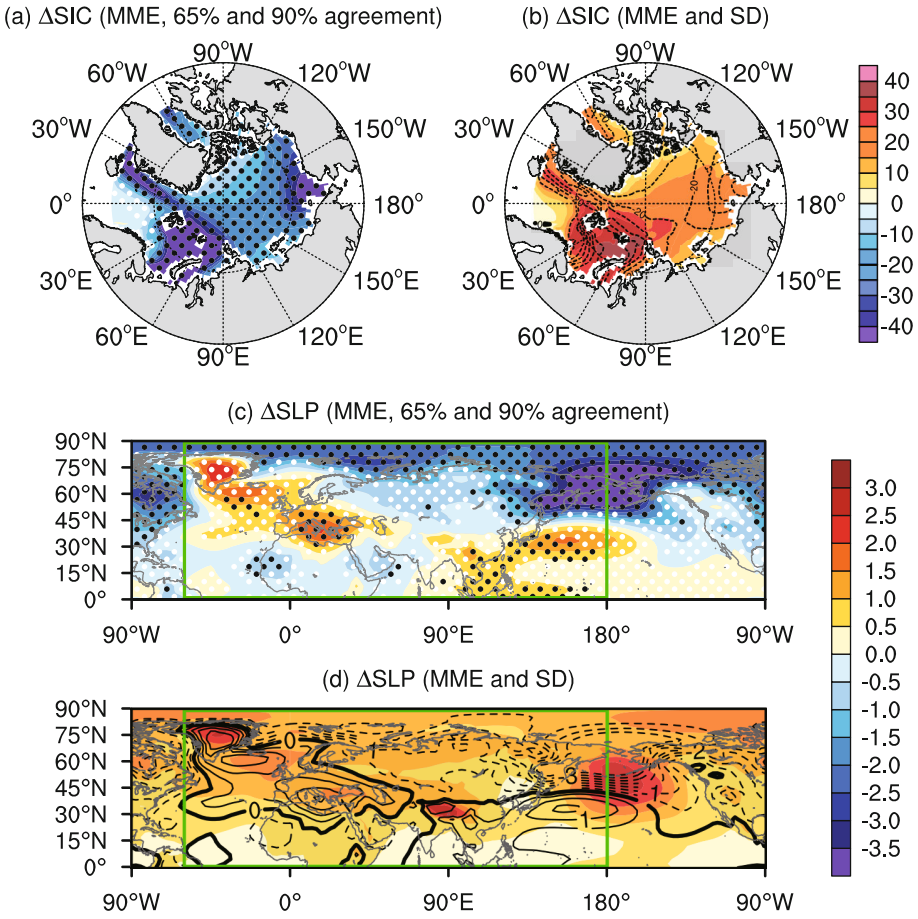


**Fig. 1.** (a, c) MME mean global warming response (2069–98 relative to 1971–2000) in DJFM and (b, d) the corresponding intermodel standard deviation of the response. (a, b) SIC (%), and (c, d) mean SLP (hPa), where the green box indicates the domain of the SVD analysis in Fig. 2. In (a) and (c), white and black dotted regions indicate at least 7 (~ 65%) and 10 (~ 90%) out of 11 models agreeing on the sign of change. In (b) and (d), contours indicate the MME mean response in (a) and (c).

North Pacific and this is associated with a stronger Aleutian low (Fig. 1c). In contrast, the SLP over the North Atlantic and Greenland increases, but there is not a large agreement among models on the sign of response (< 90%; Fig. 1c). These regions also have a large intermodel standard deviation, suggesting a large projected uncertainty of the Icelandic low and the NAO.

There is also a robust response in SLP outside the polar region. This includes an increase in SLP near the Mediterranean Sea and a decrease in SLP over western Africa (Fig. 1c), suggesting a northeastward extension of the Azores high. In addition, the SLP increases robustly over Southeast Asia and south of Japan (Fig. 1c), reflecting an expansion of the subtropical high over the western North Pacific and a northward shift of the East Asian trough. In other parts of Eurasia, the MME response of the SLP is comparable and even smaller than the intermodel standard deviation, and most models do not agree on the sign of the response (Fig. 1d). As cold air originating from the polar region strongly influences the Eurasian climate, it is important to assess the potential links between the projected uncertainties in the Arctic SIC and the Eurasian climate.

During the late 21st century, most models agree in simulating an ice-free Arctic in boreal autumn, whereas this agreement has a large spread in boreal winter. As the polar air strongly affects the lower-latitude regions, we hypothesize a simultaneous linkage between the intermodel spread of the forced response of the SIC (ΔSIC) and the Eurasian circulation in boreal winter. To test our hypothesis, we use singular value decomposition (SVD) to identify the spatial pattern accounting for the largest fraction of their covariability.

In the SVD analysis, the left-hand vector is the DJFM-mean response in (ΔSIC) over the entire Arctic, whereas the right-hand vector is the DJFM-mean SLP response (ΔSLP) over (0°–90°N, 60°W–180°), which is a domain able to capture the large-scale circulation features in Eurasia, of the 11 models. Note that the series of our SVD analysis is a time-invariant model-dependent parameter (i.e., the forced response of different models) instead of a time-varying parameter in a conventional SVD analysis, as mentioned in Bretherton et al. (1992) and Wallace et al. (1992). Therefore, the expansion coefficient of our SVD analysis is a series of 11

models instead of time steps. This approach was adopted in Wang et al. (2014), who analyzed the covariability between the biases of the global SST and the meridional overturning circulation across CMIP5 models. Note that the power of the SVD analysis here is to identify the spatial patterns accounting for the largest covariability between the model uncertainties of ΔSIC and ΔSLP, and to quantify their covariability. The coupling between these uncertainties can be due to different physical processes. This is not trivial using simpler composite or correlation analysis, which requires an index (say, the sea-ice change in the Arctic) to be first defined. Such a composite analysis cannot measure how strongly the uncertainties of ΔSIC are coupled to ΔSLP.

The first three SVD modes (SVD1-3) explain 70.5%, 16.4% and 6.63% of the total squared covariance, and hence we focus only on the first mode (SVD1). The correlation between the expansion coefficients of ΔSIC from the SVD1 and ΔSIC (the homogeneous correlation map) is shown in Fig. 2a. The spatial pattern of ΔSIC represents a strong decline in SIC over most of the Arctic, except the Barents Sea openings. Consistently, the expansion coefficient of ΔSIC is almost perfectly correlated (across the 11 models) to the DJFM-mean Arctic total sea-ice extent (the total area of grid points with SIC > 0.15) for the period 2069–98, and the difference between 2069–98 and 1971–2000 ($r = -0.97$ in both cases).

The correlation between the expansion coefficients of ΔSIC of the SVD1 and ΔSLP in Eurasia (the heterogeneous correlation map) is shown in Fig. 2b. The spatial pattern of ΔSLP consists of a north–south-oriented dipole over the Euro-Atlantic region and a strong anticyclone over the Eurasian continent (Fig. 2b). First, the positive ΔSLP over the North Atlantic suggests a weaker Icelandic low; here, models with stronger sea-ice loss reinforce the MME response (Fig. 1b). Second, the negative ΔSLP over the Mediterranean region suggests a weaker northeastward extension of the Azores high; here, models with increased sea-ice loss suppress the MME response (Fig. 1b). Such a dipole ΔSLP pattern suggests a linkage between the SVD1 and the projected difference of the NAO. Third, the signal over Asia represents a positive ΔSLP anomaly at the northwestern flank of the Siberian high, where the climatological center is located at (40°-65°N, 80°–120°E) (Panagiotopoulos et al., 2005; Fig. 2b). This is opposite in sign to the MME response.

The linkage between ΔSIC and the large-scale circulation response (Fig. 2b) could be associated with thermal interaction or a large-scale response to an eddy-mean flow interaction. To assess the relative importance of these two effects, we correlate the ΔSIC of the SVD1 to the wind response at 250 hPa (the upper troposphere) and at 850 hPa (the lower troposphere). When the linkage is related to an eddy-mean flow interaction, the atmospheric response has an equivalent barotropic structure. In contrast, the atmospheric response due to a thermal forcing has a baroclinic structure (Hoskins and Karoly, 1981; Overland and Wang, 2010; Jaiser et al., 2012). As shown in Fig. 2c, models with a stronger SIC decline exhibit lower SLP over the entire Arctic. In the lower troposphere, the associated wind response is an anticyclonic flow over the Asian side, suggesting a baroclinic response. On the other hand, the associated wind response is a cyclonic flow over the Euro-Atlantic side, suggesting an equivalent barotropic response associated with an eddy-mean flow interaction. Next, in section 3, we investigate if the atmospheric response related to the ΔSIC of the SVD1 is accompanied by forcing originating from outside of the Arctic.

## 3. Linkage to large-scale circulation

We further depict the linkage between the ΔSIC of the SVD1 and the DJFM-mean large-scale circulation features using intermodel regression, where the forced response of other variables is regressed against the standardized expansion coefficient of the left-hand vector of SVD1 (i.e., ΔSIC). All statistical analyses apply the two-tailed Student's *t*-test with the 90% confidence level.

Note that the objective of this study is to analyze the significant link between the projected uncertainties of the Arctic sea-ice decline and the Eurasian circulation. However, one may be interested to know if the intermodel response to the ΔSIC of the SVD1 has the same or opposite sign to the MME response. One may also be interested to know if the sign of these responses is in large agreement across the models. Accordingly, we also show the MME response of the large-scale parameters and highlight the regions that the models agree on the sign of the response by at least 65% and 90%, i.e., the same as Figs. 1a and b.

### 3.1. *SST and turbulent heat fluxes*

During the recent AA period, one of the potential causes of the SIC decline is the remote signals of SST originating from the tropical Pacific (Ding et al., 2014; Trenberth et al., 2014). In particular, model studies suggest the Pacific Decadal Oscillation can contribute to AA (Svendsen et al., 2017[b]; Tokinaga et al., 2017), and could modulate the response to sea-ice loss (Screen and Francis, 2016). Because part of the projected uncertainties of ΔSIC is probably linked to the forcing outside the Arctic, it is interesting to see if the ΔSIC of the SVD1 shows a strong linkage with the simultaneous response of the SST (ΔSST) and the associated turbulent heat fluxes anywhere.

As shown in Fig. 3, only the Barents–Kara Sea and the midlatitude North Atlantic have pronounced differences in DJFM-mean ΔSST associated with a stronger SIC decline. In the former region, the models robustly simulate an increase in SST and turbulent heat fluxes (Figs. 3c and d), which is related to the SIC decline. Associated with a stronger SIC decline of the SVD1, both the SST and turbulent heat fluxes have a stronger increase (Figs. 3a and b). For the second region, the majority of models simulate a weakened Atlantic meridional overturning circulation in the 21st century,

[b]Svendsen, L., N. S. Keenlyside, I. Bethke, and Y. Gao, 2017: Pacific contribution to the early 20th century warming in the Arctic. Submitted.

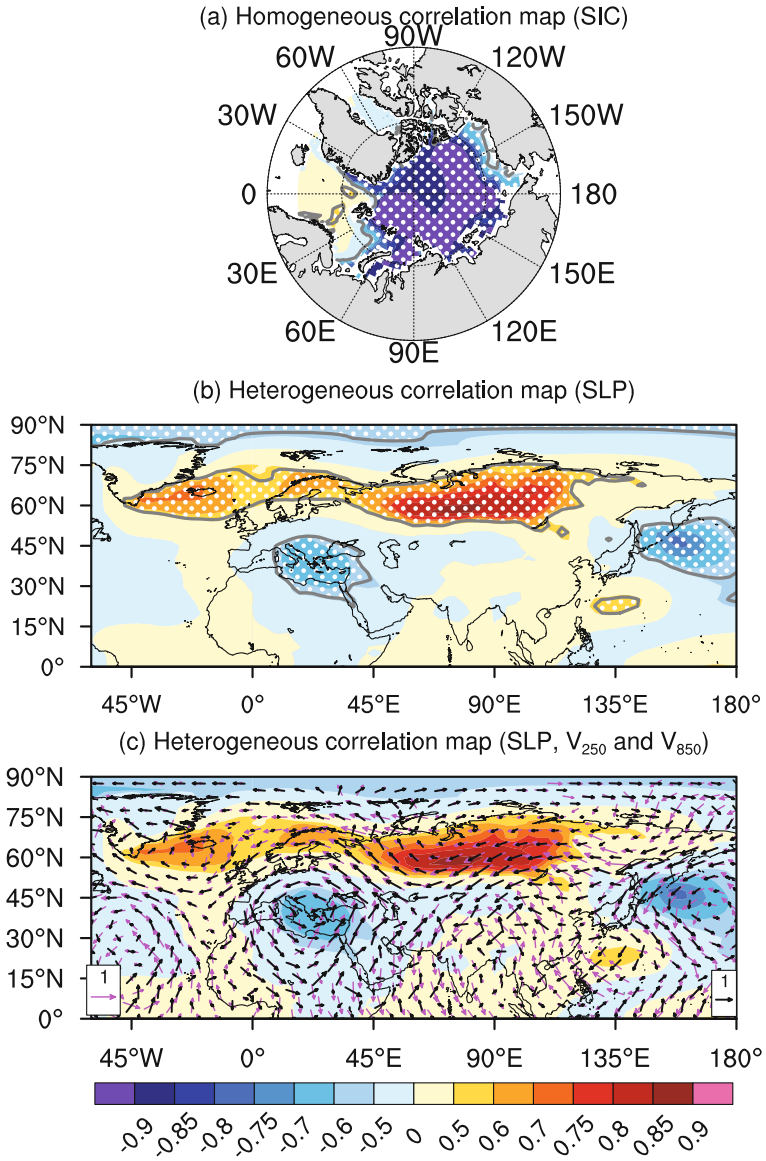


**Fig. 2.** The dominant relation between uncertainties in the global warming response in winter of sea ice and SLP over Eurasia, explaining 70% of intermodel covariability. Intermodel correlation between the expansion coefficients of the DJFM SIC response from the SVD1 and the response in DJFM-mean (a) SIC, (b) SLP, and (c) SLP (shading), 250-hPa wind (magenta arrows) and 850-hPa vector wind (black arrows); the left-hand vector and the right-hand vector of the SVD1 is the DJFM-mean change of sea-ice cover and the SLP, respectively. Thick gray lines denote $p = 0.1$; white dotted regions and vectors indicate $p < 0.1$.

although with large uncertainties in strength (Cheng et al., 2013; Collins et al., 2013; Reintges et al., 2017). Whereas the models robustly simulate a reduction of turbulent heat fluxes (Fig. 3d), they have a small agreement for the SST projection in this region (Fig. 3c). Because a stronger SIC decline of the SVD1 accompanies an anomalous SST warming in this region (Fig. 3b), the projected uncertainty of ΔSIC may be related to the Atlantic meridional overturning circulation, either through an oceanic pathway (Årthun et al., 2012) or an atmospheric connection (Sato et al., 2014). Specifically, models with stronger SST warming coincide with stronger turbulent heat fluxes locally (Fig. 3b). This is associated with a decrease in the low-level baroclinicity (figure not shown) and weaker westerly winds in the lower and upper troposphere (Fig. 2c). Therefore, the midlatitude circulation response uncertainties associated with the ΔSIC of the SVD1 could be due to both the projected uncertainties of the SIC decline and the SST warming in the North Atlantic (Woollings et al., 2012). The tropical SSTs seem to play an insignificant role in the dominant linkage between the uncertainties of sea-ice–

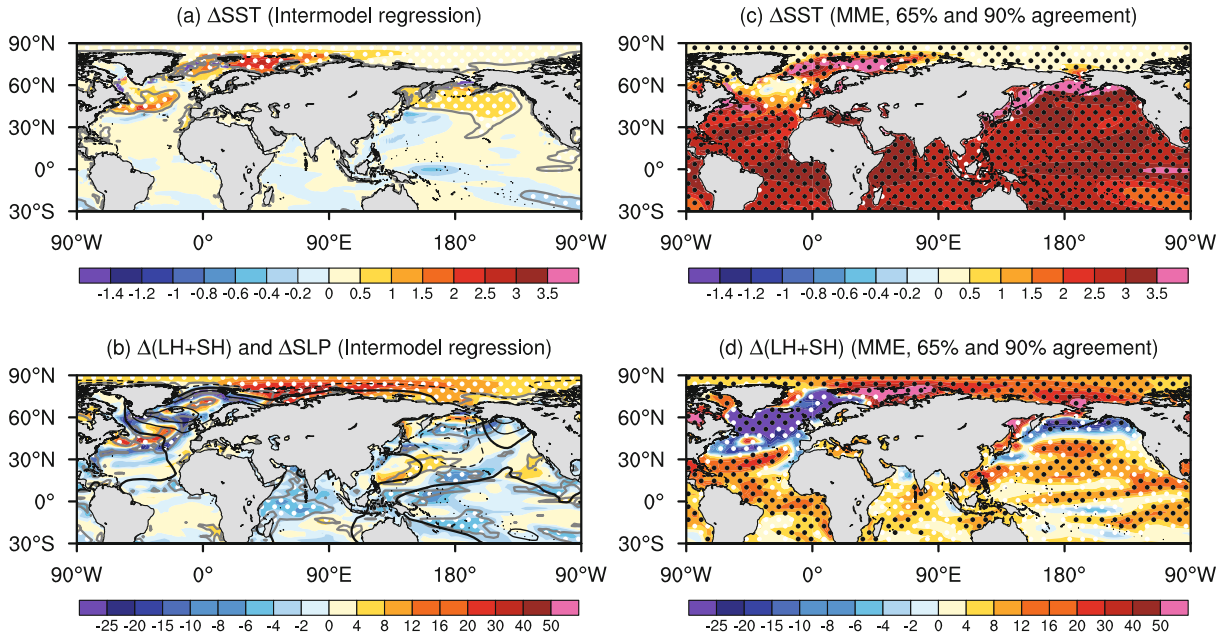


**Fig. 3.** (a, b) Intermodel regression of the forced response against the standardized expansion coefficient of SVD1 in boreal winter: (a) SST (K); (b) turbulent heat fluxes (shading; W $m^{-2}$; positive upwards) and SLP (contours; hPa). Thick gray lines denote $p = 0.1$ and dotted regions indicate $p < 0.1$ for the shaded variable. (c, d) As in (a, b) but for the MME response of the shaded terms in (a, b), where white and black dotted regions indicate at least 7 (~ 65%) and 10 (~ 90%) out of 11 models agreeing on the sign of change.

Northern Hemisphere atmospheric responses in winter.

### 3.2. *Zonal-mean circulation*

The spatial pattern of both the ΔSIC of the SVD1 and its associated turbulent heat fluxes in the polar region exhibit strong zonal wave number-0 components (Fig. 2a and Fig. 3b). Thus, we explore the linkage between the ΔSIC of the SVD1 and the DJFM zonal-mean circulation changes at different altitudes. Among the 11 models, only three are high-top models with a model top above the stratopause (Table 1). Assuming that the low-top models do not resolve the stratospheric dynamics well, we only show the composite differences up to the 100-hPa level (the lower stratosphere).

A stronger SIC decline associated with SVD1 is linked to an increased zonal-mean Arctic warming confined to the lower troposphere (Fig. 4a). Compared to the MME response, models with a stronger SIC decline (Fig. 4a) do not contribute significantly to the intermodel spread in the pronounced upper-tropospheric warming aloft in the Arctic and outside of the Arctic (Fig. 4d). This is consistent with other studies (e.g., Screen and Simmonds, 2010; Manzini et al., 2014; Blackport and Kushner, 2017; Ogawa et al., 2017[a]). Models with more pronounced lower-tropospheric warming in the Arctic than in the low-latitude region exhibit weakening of the equator-to-pole temperature gradient and midlatitude westerlies (Fig. 4b). These tropospheric circulation features are the first-order response of AA (Cohen et al., 2014; Vihma, 2014). The SVD analysis suggests the uncertainties in the MME response seen in the midlatitude westerlies (Fig. 4e) are related to pan-Arctic sea-ice decline.

The dynamical response corresponding to a stronger SIC decline of the SVD1 can be approximated by weaker tropospheric Polar and Ferrell cells, where the mass stream function response is opposite in sign to the climatology, and the boundary between these two cells shifts southward (i.e., the zero-line shifts southward; Figs. 4b and c). When less cold polar air sinks near the surface, the SLP becomes lower across the polar region (Fig. 2b). This is associated with an anomalous upward motion in the poleward branch of the Polar cell, and an anomalous downward motion in the equatorward branch of the Polar cell and the poleward branch of the Ferrell cell (Figs. 4b and c). Due to the linkage between the vertical velocity and the surface divergence, there is a stronger increase in SLP around 60°N (Fig. 2b), where the anomalous zonal-mean downward motion is strongest (Fig. 4b). At the southern flank of the positive SLP response linked to a stronger Arctic warming response (Fig. 2b and Fig. 4a), the deceleration of westerly winds is strongest (~ 50°N; Fig. 4b). This anomalous zonal-mean zonal wind response has a barotropic structure, with pronounced easterly anomalies in the upper troposphere and the lower stratosphere (Fig. 4b).

It should be noted that the models do not robustly simulate a weaker Polar cell in the lower troposphere by the end of the century (Fig. 4f), although the SIC decline is a robust signal (Fig. 1a). This suggests that the MME response (not its uncertainties) of surface circulation changes in the Arctic are also influenced by the forcing other than the sea ice, such as tropical SST forcing (e.g., Ding et al., 2014). Moreover, the models tend to simulate a strong Polar cell in the upper troposphere (Fig. 4f). Similarly, whereas the models robustly sim-

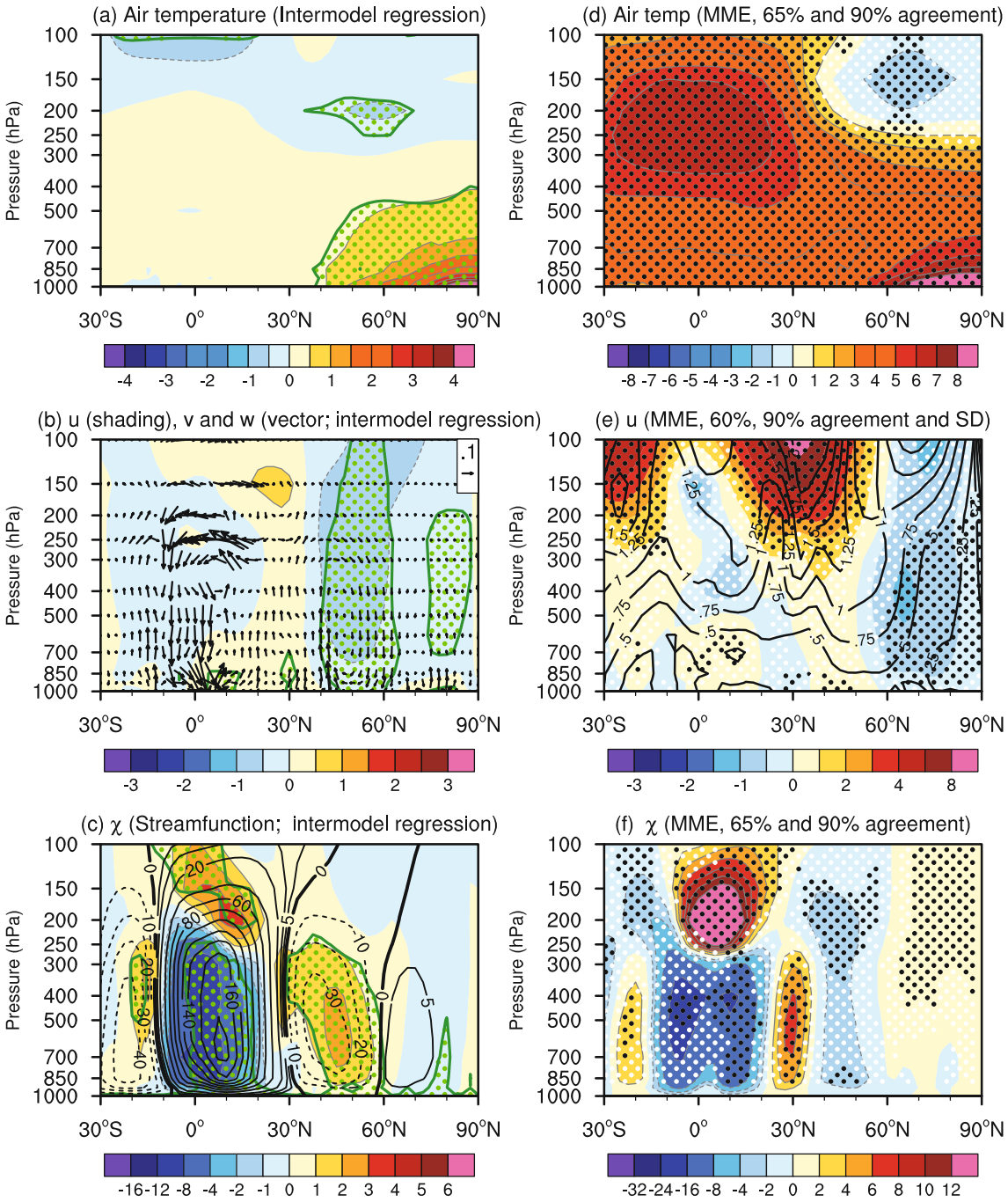


**Fig. 4.** (a–c) Latitude–height cross sections showing the intermodel regression of the forced response of the zonal-mean fields against the standardized expansion coefficient of SVD1: (a) air temperature (K); (b) zonal-mean zonal wind (shading; m $s^{-1}$) and meridional wind together with the vertical velocity (vectors; m $s^{-1}$ in the meridional direction and 0.01 Pa $s^{-1}$ in the vertical direction); (c) mass stream function ($10^9$ kg $s^{-1}$), where the black contours represent the 2069–98 climatology ($10^9$ kg $s^{-1}$). Thick green lines denote $p = 0.1$ and dotted regions have $p < 0.1$. (d–f) As in (a–c), but for the MME response of the shaded terms in (a–c), where white and black dotted regions indicate at least 7 (~ 65%) and 10 (~ 90%) out of 11 models agreeing on the sign of change. In (e), the lines represent the intermodel standard deviation (interval: 0.25 m $s^{-1}$) of the zonal-mean zonal wind change.

ulate weakening of the upper-tropospheric zonal wind aloft in the Arctic (Fig. 4e), the zonal-mean zonal wind here is slightly weakened by a stronger SIC decline of the SVD1 (Fig. 4b). Although the regressed anomalies are statistically significant, the magnitude is small compared to the MME response (Figs. 4b and e). These again suggest that the strong sea-ice decline of the SVD1 is not associated with strong upper-tropospheric circulation changes aloft in the Arctic.

In the midlatitudes, the zonal-mean zonal wind generally strengthens and this MME response is most robust near the

tropopause and in the lower stratosphere (Fig. 4e). This is due to an intensification and a northward shift of the subtropical jet in response to global warming (Seidel et al., 2008). Because the zonal-mean zonal wind response that is linked to a stronger SIC decline of the SVD1 is opposite in sign to the MME response (Figs 4b and e), the SIC-related forcing appears to weaken the global warming response. This contrast can also be seen in the mass stream function of the Ferrell cell, where the anomalous response to a stronger SIC decline of the SVD1 is positive in sign (Fig. 4c) and the MME response is negative in sign (Fig. 4f). The positive anomalous response suggests an anomalously weaker Ferrell cell (Fig. 4c), which accompanies less poleward transport of eddy momentum and heat fluxes. In addition, the intermodel spread of the zonal-mean zonal wind is largest in the stratosphere (above 100 hPa; not shown) and it extends downward into the lower troposphere (Fig. 4e). The strengthening of the midlatitude zonal-mean zonal wind in the MME response appears to be linked to the stratospheric signals, whereas the weakening of the zonal-mean zonal wind in the SVD1 is due to SIC-related signals. The former is consistent with Manzini et al. (2014), who highlighted the importance of stratospheric forcing in future surface circulation changes.

In addition to the linkage with anomalously weaker Polar and Ferrell cells, the stronger SIC decline of the SVD1 is linked to an overall weaker Hadley cell (Fig. 4c). Similar to the MME response, the anomalous response to a stronger SIC decline of the SVD1 suggests a stronger Hadley cell at its northern edge and in the upper troposphere (Fig. 4f). This represents a northward shift and a deeper Hadley cell. In short, the ΔSIC of the SVD1 is linked to the hemispheric-scale circulation in boreal winter, where the classical three-cell meridional circulations are weakened, consistent with weaker poleward heat transport (Kang et al., 2008).

### 3.3. *Eurasian circulation*

Whereas the ΔSIC of the SVD1 has a strong linkage with the projected difference of the zonal-mean circulation, it also has a zonal asymmetric component (Fig. 2a). But how strongly does it affect the intermodel agreement of the large-scale circulation features in Eurasia, including the heterogeneous SLP pattern as shown in Fig. 2b? To demonstrate these linkages, we show the intermodel regression of different large-scale atmospheric variables against the expansion coefficient of the SVD1 for the DJFM period in Fig. 5. Because the ΔSIC of the SVD1 is almost perfectly correlated to the response of the total sea-ice extent, we also define several large-scale circulation indices (Table 2) and show their scatterplot against the response of the total Arctic sea-ice extent for the DJFM period in Fig. 6.

#### 3.3.1. *Central and East Asia*

Recall that the MME of ΔSIC shows the largest decrease in SIC around the sea-ice edge, where the primary center is located at the Barents–Kara Sea (> 60%) and the secondary center is located at the Bering Strait (> 40%; Fig. 1a). The intermodel regression shows that the largest decrease north of the Kara Sea (> 50%) and the difference over the Barents Sea opening is insignificantly small (< 10%; figure not shown). The local response to stronger pan-Arctic sea-ice decline exhibits the largest increase in surface air temperature near the Kara Sea (Fig. 5a). Meanwhile, the stronger sea-ice decline leads to an increase in the water vapor content in the air column (Bintanja and Selten, 2014). This also enhances the precipitation (Fig. 5b) and decreases the vertical stability (Fig. 5d) locally. These changes reinforce the MME response (Figs. 5e–g). As the Arctic warming extends upward in the lower troposphere, the 1000–500 hPa thickness height increases and attains a maximum over the Barents-Kara Sea (~ 75°N, 50°E; Fig. 5a). This is associated with a stronger surface anticyclone over the Urals-Siberia region (~ 60°–110°E) and stronger southerly winds near the Barents Sea (Fig. 5b).

**Table 2.** List of large-scale circulation indices that are plotted in Fig. 6.

| Index | Definition |
|---|---|
| Urals–Siberia SLP | Area-averaged SLP over (55°–65°N, 60°–90°E) |
| Icelandic low index | Area-averaged SLP over (55°–67.5°N, 35°–15°W) |
| Mediterranean SLP | Area-averaged SLP over (30°–45°N, 10°–35°E) |
| NAO | The first EOF pattern obtained from the monthly SLP covariance matrix over (20°–80°N, 90°W–40°E) in the NCEP–NCAR reanalysis datasets. |

The intermodel correlation between the SLP response over the Urals–Siberia region and the pan-Arctic sea-ice decline is −0.752 (~ 57% of the total variance; Fig. 6a). The SIC signals of the SVD1 appear to modulate instead of dominate the SLP response, as most models (9 out of 11) simulate a negative SLP response over this region (Fig. 6a). The anticyclone related to the increased SIC decline extends across the whole of northern Asia. Whereas the stronger anticyclone likely strengthens the northerly cold-air advection, the meridional temperature gradient over the high-latitude region sharply decreases and this weakens the northerly cold-air advection (Fig. 5c). Hence, it is unclear if the seasonal-mean cold-air advection is strengthened by a larger sea-ice decline of SVD1. Note that correlation analysis does not imply any causality of the linkage (i.e., increased Arctic SIC decline could instead be driven by the Eurasian SLP changes, or both the sea ice and SLP might be independently affected by a third factor).

The anomalous surface air temperature response of the SVD1 shows a more pronounced warming spread across the high-latitude region of Asia (Fig. 5e), whereas part of the Siberian–Mongolian region (~ 40°–55°N, 90°–120°E) has a slight and insignificant "cooling" associated with the SVD1 [note that this "cooling" means the warming is less pronounced, as the magnitude of the intermodel regression is much smaller than the MME response (Figs. 5a and e). The

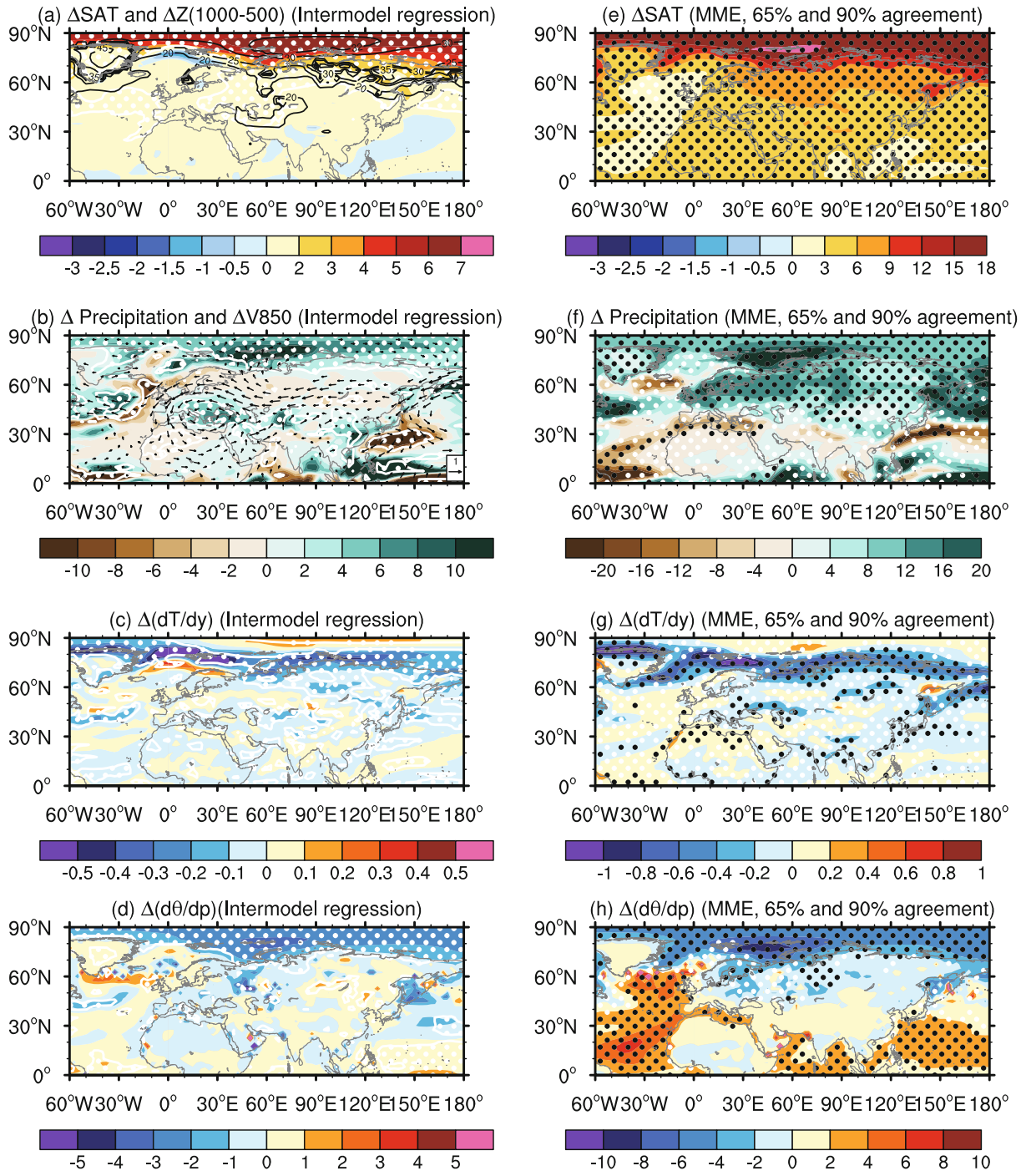


**Fig. 5.** Intermodel regression against the standardized expansion coefficient of SVD1 in DJFM: (a) surface air temperature (shading; K) and thickness height between 1000 and 500 hPa; (b) precipitation (shading; mm month$^{-1}$) and 850-hPa wind (black vectors; m s$^{-1}$), (c) meridional surface air temperature gradient ($10^{-5}$ K m$^{-1}$); (d) vertical stability at 925 hPa (K hPa$^{-1}$). Thick white lines denote $p = 0.1$ and dotted regions and vectors have $p < 0.1$. (e–h) As in (a–d) but for the MME response of the shaded terms in (a–d), where white and black dotted regions indicate at least 7 (~ 65%) and 10 (~ 90%) out of 11 models agreeing on the sign of change.

stronger increase in temperature over northern Asia (Fig. 5a) is mainly due to the stronger reduction in the meridional temperature gradient (Fig. 5c). Part of the stronger warming over Northeast Asia (~ 100°–140°E) is related to the increase in vertical stability (Fig. 5d). The change in the downwelling shortwave radiation and the turbulent heat fluxes play an insignificant role (figure not shown).

### 3.3.2. *Euro-Atlantic region*

Over the Euro-Atlantic region, the intermodel regression against the SVD1 projects on to a negative NAO-like dipole pattern, with an anomalous high near Iceland, weak anoma-

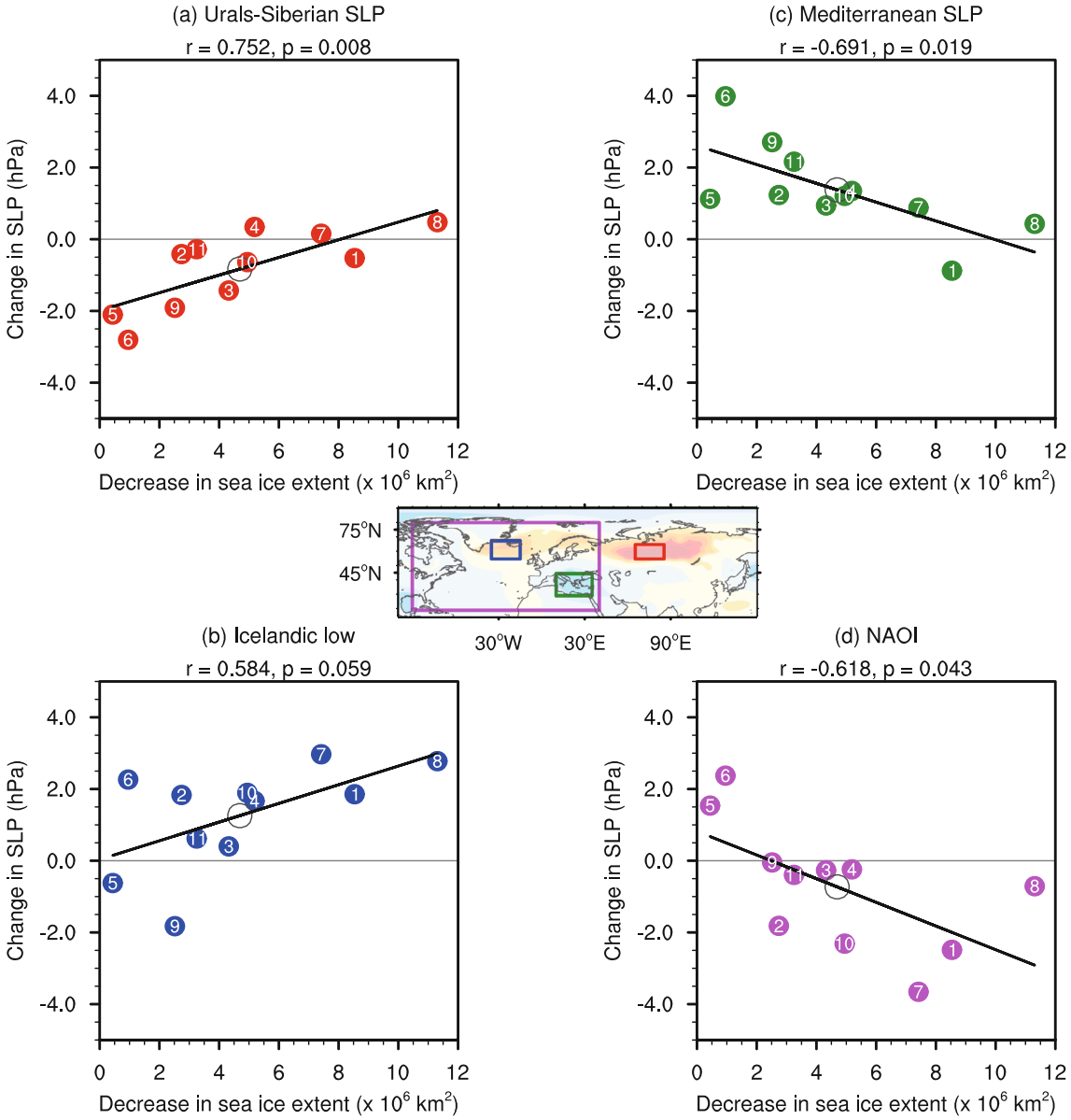


**Fig. 6.** Scatterplots of the forced response of large-scale circulation indices against the decrease in sea-ice extent in DJFM: (a) Urals–Siberia SLP; (b) Icelandic low index; (c) Mediterranean SLP; (d) NAO index. In each plot, the number denotes the response of individual models listed in Table 1, whereas the open circle represents the MME response. The correlation of the intermodel regression line (thick solid line) and the corresponding level of significance are shown at the top.

lies over the subtropical Atlantic, and an anomalous low near the Mediterranean Sea (Fig. 2b). On the one hand, the majority of models (9 out of 11) simulate a weaker Icelandic low that is intensified in models simulating a stronger sea-ice decline of the SVD1 (Fig. 6b). A stronger sea-ice decline is associated with a weaker Polar cell and anomalous downward motion near 60°N (Fig. 4b), which is close to the center of action of the Icelandic low. Moreover, a stronger sea-ice decline of the SVD1 is accompanied by a stronger Arctic warming and a smaller equator-to-pole temperature gradient. According to Harvey et al. (2015), this is related to the lower tropospheric baroclinicity and is hence crucial for reducing the storm tracks in the northern North Atlantic (see their Fig. 5c). As the sea-ice decline is a robust feature in the future climate, the increase in SLP near the Icelandic low region appears to be linked to the storm track changes. Under a stronger SIC decline of the SVD1, the meridional surface temperature gradient becomes weaker along the Gulf Stream (Fig. 5c). As can also be seen in Fig. 5b, this accompanies an anomalous anticyclonic flow and negative precipitation anomalies extending northeastward from Iceland toward Scandinavia. All the aforementioned features suggest a further reduction in the Northeastern Atlantic storm tracks (Rogers, 1997), which needs to be investigated in future studies.

On the other hand, all but one of the models simulate an

increase in SLP in Mediterranean Europe (Fig. 6c), and this response is strongly suppressed by a stronger SIC decline of the SVD1 (Fig. 2b). As can be inferred from Fig. 5b, a stronger sea-ice decline is associated with an anomalous cyclonic flow over the tropical and subtropical North Atlantic. The Azores high might have a smaller northeastward extension toward Mediterranean Europe, where the SLP robustly increases (Fig. 1c). This anomalous response can be regarded as a weaker Hadley cell (Fig. 4c), where the intermodel correlation between the zonal-mean mass stream function averaged over 10°–20°N in the 850–500 hPa levels and the SLP over Mediterranean Europe is +0.872. The anomalous low over Mediterranean Europe is associated with a stronger southerly advection of the warm subtropical air toward southeastern Europe. This accompanies an anomalous increase in surface air temperature and precipitation over part of Central Europe, Mediterranean Europe and the Middle East (Figs. 5a and b).

Because a stronger pan-Arctic sea-ice decline is linked to weakening of the Icelandic low but little change to the intensity of the Azores high, it has a significant negative correlation with the NAO response (Fig. 6d). However, it is noticeable that the NAO response does not robustly show a negative tendency. The spread is consistent with the inconsistency of the NAO response among previous studies (Vihma, 2014), suggesting other factors also affecting the NAO change. Moreover, the stronger negative NAO response does not correspond to a colder and even a less warm climate over Europe (Fig. 5a). Altogether, a stronger pan-Arctic sea-ice decline in boreal winter might significantly modulate the key circulation features over Eurasia, where the anomalous SLP and precipitation responses (Fig. 2b and Fig. 5b) are often opposite in sign to the MME response (Fig. 1c and Fig. 5f). However, an anomalous high does not correspond to anomalous cooling, unlike the warm-Arctic–cold-Eurasia temperature pattern during the recent AA period (e.g., Cohen et al., 2014).

## 4. Summary and discussion

We have demonstrated strong linkages between the intermodel spread of the pan-Arctic sea-ice decline and the Eurasian climate. The linkages explain 70.5% of the total variance, when represented by the joint SVD1 mode of the Arctic SIC (as the left-hand vector) and the Eurasian SLP (as the right-hand vector). The intermodel spread of the Arctic SIC is significantly linked to the MME response of the Eurasian climate, including (1) the SLP over the Eurasian continent, (2) the Icelandic low and possibly the northeastern Atlantic storm tracks, (3) the SLP over Mediterranean Europe, and (4) the eastward shift of the NAO-like response.

Our results suggest that a stronger Arctic sea-ice decline of the SVD1 is associated with an anomalous increase in SLP over high-latitude Eurasia, including the Urals–Siberia region and the Icelandic low region. However, we did not find significantly stronger northerly winds over Eurasia. Nor did we find any cooling or even less pronounced warming in any part of Eurasia. This is different from the present climate, where a stronger high pressure and persistent snow cover over Eurasia might enhance the upward propagation of the planetary waves from the troposphere to the stratosphere (e.g., Allen and Zender, 2011; Cohen et al., 2012; Kim et al., 2014). One possible reason is that only 3 out of the 11 models have a well-resolved stratosphere, which is crucial for simulating the midlatitude atmospheric response associated with the troposphere–stratosphere interaction (Omrani et al., 2014, 2016; Nakamura et al., 2015; Zhang et al., 2017).

Other possible reasons are that the impact of the pan-Arctic sea-ice loss is different from the regional sea-ice loss (Screen, 2017), or the recent changes are dominated by internal atmospheric variability (McCusker et al., 2016; Ogawa et al., 2017[a]). Regarding the former factor, a stronger anticyclone over high-latitude Eurasia driven by a regional sea-ice decline over the Barents–Kara Sea could enhance the downstream cold-air advection, as the sea ice is still present downstream. The resultant dynamic effect of regional sea-ice loss could cause cooling in the mid and high latitudes (Mori et al., 2014; Kug et al., 2015; Overland et al., 2015).

Conversely, in response to the pan-Arctic sea-ice loss, the cold-air intensity over the entire Arctic becomes weaker. The meridional temperature gradient in the high latitudes decreases and the midlatitude westerlies weaken. Unless the northerly winds become much stronger (such as a higher amplitude flow), the northerly cold-air advection would be weaker. Screen (2014) also suggested that the northerly wind makes a larger contribution to the warming trend in the high-latitude region than the southerly wind during boreal winter. Recently, Meleshko et al. (2016) showed that the ocean heat transport is more important for the higher amplitude planetary wave in the midlatitudes. Based on these findings, it is unlikely that the pan-Arctic sea-ice loss causes any cooling effect in the extratropical region on seasonal timescales, which agrees with the results of Deser et al. (2016) and Screen (2017).

A stronger Arctic sea-ice decline of the SVD1 is also linked to weakening of the three-cell circulations and a warmer SST in the midlatitude North Atlantic. In the midlatitudes, a weaker Ferrell cell is characterized by a higher SLP in the midlatitudes and weaker zonal-mean zonal winds. However, we cannot assess the causality of these linkages. Indeed, the stronger SST warming over the North Atlantic could enhance the poleward ocean heat transport and could then melt more sea ice (Mahlstein and Knutti, 2011; Jung et al., 2017; Nummelin et al., 2017). The basin-wide Atlantic warming is also crucial for the negative tendency of the NAO, via an atmospheric wave train (Sato et al., 2014) and troposphere–stratosphere interaction (Omrani et al., 2016). The atmospheric response to the sea-ice decline might also be highly nonlinear (Petoukhov and Semenov, 2010). In a future study, we intend to design several sensitivity experiments based on the intermodel spread of SST and SIC, in order to assess the relative importance of these projected uncertainties in the future climate change of the Northern Hemisphere.

***Acknowledgements.*** The work of HC, NK and NO was supported by grants from the European Research Council (ERC) project (Grant No. 648982) and NordForsk under the GREENICE (Grant No. 61841) and ARCPATH (Grant No. 76654) projects, and the work of WZ was supported by grants from the Research Grants Council of the Hong Kong Special Administrative Region, China (CityU 11335316 and 11305715). The authors also benefit from high performance computing grants (NOTUR2, project no. NN 9390K; NORSTORE, NS9064K). The authors acknowledge the World Climate Research Programme's Working Group on Coupled Modelling, which is responsible for CMIP, and we thank the climate modeling groups (listed in Table 1 of this paper) for producing and making available their model output. We also greatly appreciate the valuable comments given by the two anonymous reviewers, which helped improve the clarity of our results.



## REFERENCES

Allen, R. J., and C. S. Zender, 2011: Forcing of the Arctic Oscillation by Eurasian snow cover. *J. Climate*, **24**, 6528–6539, https://doi.org/10.1175/2011JCLI4157.1.

Årthun, M., T. Eldevik, L. H. Smedsrud, Ø. Skagseth, and R. B. Ingvaldsen, 2012: Quantifying the influence of Atlantic heat on Barents Sea ice variability and retreat. *J. Climate*, **25**, 4736–4743, https://doi.org/10.1175/JCLI-D-11-00466.1.

Ayarzagüena, B., and J. A. Screen, 2016: Future Arctic sea ice loss reduces severity of cold air outbreaks in midlatitudes. *Geophys. Res. Lett.*, **43**, 2801–2809, https://doi.org/10.1002/2016GL068092.

Barnes, E. A., and L. M. Polvani, 2015: CMIP5 projections of Arctic amplification, of the North American/North Atlantic circulation, and of their relationship. *J. Climate*, **28**, 5254–5271, https://doi.org/10.1175/JCLI-D-14-00589.1.

Barnes, E. A., and J. A. Screen, 2015: The impact of Arctic warming on the midlatitude jet-stream: Can it? Has it? Will it? *WIREs Climate Change*, **6**, 277–286, https://doi.org/10.1002/wcc.337.

Bintanja, R., and F. M. Selten, 2014: Future increases in Arctic precipitation linked to local evaporation and sea-ice retreat. *Nature*, **509**, 479–482, https://doi.org/10.1038/nature13259.

Blackport, R., and P. J. Kushner, 2017: Isolating the atmospheric circulation response to Arctic sea ice loss in the coupled climate system. *J. Climate*, **30**, 2163–2185, https://doi.org/10.1175/JCLI-D-16-0257.1.

Bretherton, C. S., C. Smith, and J. M. Wallace, 1992: An intercomparison of methods for finding coupled patterns in climate data. *J. Climate*, **5**, 541–560, https://doi.org/10.1175/1520-0442(1992)005<0541:AIOMFF>2.0.CO;2.

Chang, C.-P., Z. Wang, and H. Hendon, 2006: The Asian winter monsoon. *The Asian Monsoon*, B. Wang, Ed., Springer, 89–127.

Chen, H. W., F. Q. Zhang, and R. B. Alley, 2016: The robustness of midlatitude weather pattern changes due to Arctic sea ice loss. *J. Climate*, **29**, 7831–7849, https://doi.org/10.1175/JCLI-D-16-0167.1.

Cheng, W., J. C. H. Chiang, and D. X. Zhang, 2013: Atlantic Meridional Overturning Circulation (AMOC) in CMIP5 models: RCP and historical simulations. *J. Climate*, **26**, 7187–7197, https://doi.org/10.1175/JCLI-D-12-00496.1.

Cohen, J. L., J. C. Furtado, M. A. Barlow, V. A. Alexeev, and J. E. Cherry, 2012: Arctic warming, increasing snow cover and widespread boreal winter cooling. *Environmental Research Letters*, **7**, 014007, https://doi.org/10.1088/1748-9326/7/1/014007.

Cohen, J. L., and Coauthors, 2014: Recent Arctic amplification and extreme mid-latitude weather. *Nature Geoscience*, **7**, 627–637, https://doi.org/10.1038/NGEO2234.

Collins, M., and Coauthors, 2013: Long-term climate change: Projections, commitments and irreversibility. *Climate Change* 2013: *The Physical Science Basis. Contribution of Working Group I to the Fifth Assessment Report of the Intergovernmental Panel on Climate Change*, T. F. Stocker et al., Eds., Cambridge University Press, 1029–1136.

Deser, C., R. Tomas, M. Alexander, and D. Lawrence, 2010: The seasonal atmospheric response to projected Arctic sea ice loss in the late twenty-first century. *J. Climate*, **23**, 333–351, https://doi.org/10.1175/2009JCLI3053.1.

Deser, C., L. T. Sun, R. A. Tomas, and J. Screen, 2016: Does ocean coupling matter for the northern extratropical response to projected Arctic sea ice loss? *Geophys. Res. Lett.*, **43**, 2149–2157, https://doi.org/10.1002/2016GL067792.

Ding, Q. H., J. M. Wallace, D. S. Battisti, E. J. Steig, A. J. E. Gallant, H.-J. Kim, and L. Geng, 2014: Tropical forcing of the recent rapid Arctic warming in northeastern Canada and Greenland. *Nature*, **509**, 209–212, https://doi.org/10.1038/nature13260.

Ding, Y. H., 1994: *Monsoons over China*. Kluwer Academic Publishers, 420 pp.

Gao, Y. Q., and Coauthors, 2015: Arctic sea ice and Eurasian climate: A review. *Adv. Atmos. Sci.*, **32**, 92–114, https://doi.org/10.1007/s003946-014-0009-6.

Graversen, R. G., T. Mauritsen, M. Tjernström, E. Källén, and G. Svensson, 2008: Vertical structure of recent Arctic warming. *Nature*, **451**, 53–56, https://doi.org/10.1038/nature06502.

Harvey, B. J., L. C. Shaffrey, and T. J. Woollings, 2015: Deconstructing the climate change response of the Northern Hemisphere wintertime storm tracks. *Climate Dyn.*, **45**, 2847–2860, https://doi.org/10.1007/s00382-015-2510-8.

Hodson, D. L. R., S. P. E. Keeley, A. West, J. Ridley, E. Hawkins, and H. T. Hewitt, 2013: Identifying uncertainties in Arctic climate change projections. *Climate Dyn.*, **40**, 2849–2865, https://doi.org/10.1007/s00382-012-1512-z.

Honda, M., J. Inoue, and S. Yamane, 2009: Influence of low Arctic sea-ice minima on anomalously cold Eurasian winters. *Geophys. Res. Lett.*, **36**, L08707, https://doi.org/10.1029/2008GL037079.

Hoskins, B. J., and D. J. Karoly, 1981: The steady linear response of a spherical atmosphere to thermal and orographic forcing. *J. Atmos. Sci.*, **38**, 1179–1196, https://doi.org/10.1175/1520-0469(1981)038<1179:TSLROA>2.0.CO;2.

Jaiser, R., K. Dethloff, D. Handorf, A. Rinke, and J. Cohen, 2012: Impact of sea ice cover changes on the Northern Hemisphere atmospheric winter circulation. *Tellus A*, **64**, 11595,

https://doi.org/10.3402/tellusa.v64i0.11595.

Jung, O., M.-K. Sung, K. Sato, Y.-K. Lim, S.-J. Kim, E.-H. Baek, and B.-M. Kim, 2017: How does the SST variability over the western North Atlantic Ocean control Arctic warming over the Barents-Kara Seas? *Environmental Research Letters*, **12**, 034021, https://doi.org/10.1088/1748-9326/aa5f3b.

Kang, S. M., I. M. Held, D. M. W. Frierson, and M. Zhao, 2008: The response of the ITCZ to extratropical thermal forcing: Idealized slab-ocean experiments with a GCM. *J. Climate*, **21**, 3521–3532, https://doi.org/10.1175/2007JCLI2146.1.

Kim, B.-M., and Coauthors, 2014: Weakening of the stratospheric polar vortex by Arctic sea-ice loss. *Nature Communications*, **5**, 4646, https://doi.org/10.1038/ncomms5646.

King, M. P., M. Hell, and N. Keenlyside, 2016: Investigation of the atmospheric mechanisms related to the autumn sea ice and winter circulation link in the Northern Hemisphere. *Climate Dyn.*, **46**, 1185–1195, https://doi.org/10.1007/s00382-015-2639-5.

Kug, J.-S., J.-H. Jeong, Y.-S. Jang, B.-M. Kim, C. K. Folland, S.-K. Min, and S.-W. Son, 2015: Two distinct influences of Arctic warming on cold winters over North America and East Asia. *Nature Geoscience*, **8**, 759–762, https://doi.org/10.1038/ngeo2517.

Magnusdottir, G., C. Deser, and R. Saravanan, 2004: The effects of North Atlantic SST and sea ice anomalies on the winter circulation in CCM3. Part I: Main features and storm track characteristics of the response. *J. Climate*, **17**, 857–876, https://doi.org/10.1175/1520-0442(2004)017<0857:TEONAS>2.0.CO;2.

Mahlstein, I., and R. Knutti, 2011: Ocean heat transport as a cause for model uncertainty in projected Arctic warming. *J. Climate*, **24**, 1451–1460, https://doi.org/10.1175/2010JCLI3713.1.

Manzini, E., and Coauthors, 2014: Northern winter climate change: Assessment of uncertainty in CMIP5 projections related to stratosphere-troposphere coupling. *J. Geophys. Res.*, **119**, 7979–7998, https://doi.org/10.1002/2013JD021403.

McCusker, K. E., J. C. Fyfe, and M. Sigmond, 2016: Twenty-five winters of unexpected Eurasian cooling unlikely due to Arctic sea-ice loss. *Nature Geoscience*, **9**, 838–843, https://doi.org/10.1038/ngeo2820.

Meleshko, V. P., O. M. Johannessen, A. V. Baidin, T. V. Pavlova, and V. A. Govorkova, 2016: Arctic amplification: Does it impact the polar jet stream? *Tellus A*, **68**, 32330, https://doi.org/10.3402/tellusa.v68.32330.

Mori, M., M. Watanabe, H. Shiogama, J. Inoue, and M. Kimoto, 2014: Robust Arctic sea-ice influence on the frequent Eurasian cold winters in past decades. *Nature Geoscience*, **7**, 869–873, https://doi.org/10.1038/ngeo2277.

Nakamura, T., K. Yamazaki, K. Iwamoto, M. Honda, Y. Miyoshi, Y. Ogawa, and J. Ukita, 2015: A negative phase shift of the winter AO/NAO due to the recent Arctic sea-ice reduction in late autumn. *J. Geophys. Res.*, **120**, 3209–3227, https://doi.org/10.1002/2014JD022848.

Nummelin, A., C. Li, and P. J. Hezel, 2017: Connecting ocean heat transport changes from the midlatitudes to the Arctic Ocean. *Geophys. Res. Lett.*, **44**, 1899–1908, https://doi.org/10.1002/2016GL071333.

Omrani, N.-E., J. Bader, N. S. Keenlyside, and E. Manzini, 2016: Troposphere-stratosphere response to large-scale North Atlantic Ocean variability in an atmosphere/ocean coupled model. *Climate Dyn.*, **46**, 1397–1415, https://doi.org/10.1007/s00382-015-2654-6.

Omrani, N.-E., N. S. Keenlyside, J. Bader, and E. Manzini, 2014: Stratosphere key for wintertime atmospheric response to warm Atlantic decadal conditions. *Climate Dyn.*, **42**, 649–663, https://doi.org/10.1007/S00382-013-1860-3.

Overland, J. E., and M. Y. Wang, 2010: Large-scale atmospheric circulation changes are associated with the recent loss of Arctic sea ice. *Tellus A*, **62**, 1–9, https://doi.org/10.1111/j.1600-0870.2009.00421.x.

Overland, J., J. A. Francis, R. Hall, E. Hanna, S.-J. Kim, and T. Vihma, 2015: The melting Arctic and midlatitude weather patterns: Are they connected? *J. Climate*, **28**, 7917–7932, https://doi.org/10.1175/JCLI-D-14-00822.1.

Panagiotopoulos, F., M. Shahgedanova, A. Hannachi, and D. B. Stephenson, 2005: Observed trends and teleconnections of the Siberian high: A recently declining center of action. *J. Climate*, **18**, 1411–1422, https://doi.org/10.1175/JCLI3352.1.

Peings, Y., and G. Magnusdottir, 2014: Response of the wintertime Northern Hemisphere atmospheric circulation to current and projected Arctic sea ice decline: A numerical study with CAM5. *J. Climate*, **27**, 244–264, https://doi.org/10.1175/JCLI-D-13-00272.1.

Petoukhov, V., and V. A. Semenov, 2010: A link between reduced Barents-Kara sea ice and cold winter extremes over northern continents. *J. Geophys. Res.*, **115**, D21111, https://doi.org/10.1029/2009JD013568.

Reintges, A., T. Martin, M. Latif, and N. S. Keenlyside, 2017: Uncertainty in twenty-first century projections of the Atlantic Meridional Overturning Circulation in CMIP3 and CMIP5 models. *Climate Dyn.*, **49**, 1495–1511, https://doi.org/10.1007/s00382-016-3180-x.

Sato, K., J. Inoue, and M. Watanabe, 2014: Influence of the Gulf Stream on the Barents Sea ice retreat and Eurasian coldness during early winter. *Environmental Research Letters*, **9**, 084009, https://doi.org/10.1088/1748-9326/9/8/084009.

Rogers, J. C., 1997: North Atlantic storm track variability and its association to the North Atlantic Oscillation and climate variability of Northern Europe. *J. Climate*, **10**, 1635–1647, https://doi.org/10.1175/1520-0442(1997)010<1635:NASTVA>2.0.CO;2.

Screen, J. A., 2014: Arctic amplification decreases temperature variance in northern mid- to high-latitudes. *Nat. Clim. Change*, **4**, 577–582, https://doi.org/10.1038/nclimate2268.

Screen, J. A., 2017: Simulated atmospheric response to regional and pan-Arctic sea ice loss. *J. Climate*, **30**, 3945–3962, https://doi.org/10.1175/JCLI-D-16-0197.1.

Screen, J. A., and I. Simmonds, 2010: The central role of diminishing sea ice in recent Arctic temperature amplification. *Nature*, **464**, 1334–1337, https://doi.org/10.1038/nature09051.

Screen, J. A., and J. A. Francis, 2016: Contribution of sea-ice loss to Arctic amplification is regulated by Pacific Ocean decadal variability. *Nat. Clim. Change*, **6**, 856–860, https://doi.org/10.1038/nclimate3011.

Seidel, D. J., Q. Fu, W. J. Randel, and T. J. Reichler, 2008: Widening of the tropical belt in a changing climate. *Nature Geoscience*, **1**, 21–24, https://doi.org/10.1038/ngeo.2007.38.

Sokolova, E., K. Dethloff, A. Rinke, and A. Benkel, 2007: Planetary and synoptic scale adjustment of the Arctic atmosphere to sea ice cover changes. *Geophys. Res. Lett.*, **34**, L17816, https://doi.org/10.1029/2007GL030218.

Sorokina, S. A., C. Li, J. J. Wettstein, and N. G. Kvamstø, 2016: Observed atmospheric coupling between Barents sea ice and

the warm-Arctic cold-Siberian anomaly pattern. *J. Climate*, **29**, 495–511, https://doi.org/10.1175/JCLI-D-15-0046.1.

Thompson, D. W. J., and J. M. Wallace, 1998: The Arctic Oscillation signature in the wintertime geopotential height and temperature field. *Geophys. Res. Lett.*, **25**, 1297–1300, https://doi.org/10.1029/98GL00950.

Tokinaga, H., S.-P. Xie, and H. Mukougawa, 2017: Early 20th-century Arctic warming intensified by Pacific and Atlantic multidecadal variability. *Proc. Nat. Acad. Sci*, **114**, 6227–6232, https://doi.org/10.1073/pnas.1615880114.

Trenberth, K. E., J. T. Fasullo, G. Branstator, and A. S. Phillips, 2014: Seasonal aspects of the recent pause in surface warming. *Nat. Clim. Change*, **4**, 911–916, https://doi.org/10.1038/nclimate2341.

Vihma, T., 2014: Effects of Arctic sea ice decline on weather and climate: A review. *Surveys in Geophysics*, **35**, 1175–1214, https://doi.org/10.1007/s10712-014-92824-0.

Wallace, J. M., C. Smith, and C. S. Bretherton, 1992: Singular value decomposition of wintertime sea surface temperature and 500-mb height anomalies. *J. Climate*, **5**, 561–576, https://doi.org/10.1175/1520-0442(1992)005<0561:SVDOWS>2.0.CO;2.

Wang, C. Z., L. P. Zhang, S.-K. Lee, L. X. Wu, and C. R. Mechoso, 2014: A global perspective on CMIP5 climate model biases. *Nat. Clim. Change*, **4**, 201–205, https://doi.org/10.1038/NCLIMATE2118.

Wang, M. Y., and J. E. Overland, 2012: A sea ice free summer Arctic within 30 years: An update from CMIP5 models. *Geophys. Res. Lett.*, **39**, L18501, https://doi.org/10.1029/2012GL052868.

Woollings, T., J. M. Gregory, J. G. Pinto, M. Reyers, and D. J. Brayshaw, 2012: Response of the North Atlantic storm track to climate change shaped by ocean-atmosphere coupling. *Nature Geoscience*, **5**, 313–317, https://doi.org/10.1038/ngeo1438.

Yang, S. T., and J. H. Christensen, 2012: Arctic sea ice reduction and European cold winters in CMIP5 climate change experiments. *Geophys. Res. Lett.*, **39**, L20707, https://doi.org/10.1029/2012GL053338.

Zhang, P. F., Y. T. Wu, and K. L. Smith, 2017: Prolonged effect of the stratospheric pathway in linking Barents-Kara Sea sea ice variability to the midlatitude circulation in a simplified model. *Climate Dyn.*, https://doi.org/10.1007/s00382-017-3624-y. (in press)